buildings

MDPI

Article

Impact of Construction Material Properties Variability on the Seismic Fragility Assessment of RC Structures in Bucharest

Florin Pavel * and Lucian Petru Florescu

Department of Reinforced Concrete Structures, Technical University of Civil Engineering Bucharest, Bd. Lacul Tei, 122-124, Sector 2, 020396 Bucharest, Romania
* Correspondence: florin.pavel@utcb.ro

Abstract

This study investigates how historical variability in construction materials influences the seismic fragility of reinforced concrete (RC) buildings in Bucharest. Mechanical properties of reinforcing steels (OB37, TOR47, and PC52) and concretes used between 1950 and 2000 are statistically characterized using archival records and experimental data. The analysis highlights significant discrepancies between prescribed and in situ concrete strengths, as well as substantial differences in ductility, overstrength, and strength variability among historical steel types. To evaluate structural implications, a representative 11-storey pre-1970 RC building is modeled using nonlinear static and incremental dynamic analysis. The results show markedly lower capacity and higher fragility in the transversal direction. Time-dependent deterioration is examined by incorporating carbonation-induced reinforcement corrosion using FIB-based formulations. Even moderate corrosion leads to measurable reductions in stiffness, ductility, and lateral capacity, producing higher fragility across all considered damage states. Seismic loss estimations further demonstrate an increase in expected annual losses for both principal directions when corrosion is considered. The findings underscore the need for era-specific material models and deterioration mechanisms to achieve accurate seismic vulnerability assessments of Bucharest's aging RC building stock.

Keywords: nonlinear analysis; seismic damage; reinforcing steel; Vrancea intermediate-depth earthquakes; concrete carbonation: reinforcement corrosion

1. Introduction

Accurate characterization of construction material properties, including monotonic and cyclic (hysteretic) stress–strain behavior, is fundamental to the reliable seismic vulnerability assessment of existing structures. Such quantification enables the development of realistic nonlinear models that capture degradation mechanisms, stiffness reduction, and energy dissipation capacity under earthquake loading. Understanding the historical evolution of construction materials is essential, as the mechanical properties of both concrete and reinforcing steel have changed significantly across decades due to variations in manufacturing processes, quality control practices, and available technologies. These material transitions directly influence the seismic performance of RC structures and must therefore be explicitly considered in vulnerability modeling.

The recent study by Pavel et al. [1] synthesizes the evolution of reinforced concrete design practices in Romania, including moment frames, shear walls, and large panel systems, and examines how material, detailing, and economic constraints have shaped their seismic

Academic Editors: Jieqiong Wu, Renbo Zhang and Shenggang Chen

Received: 26 February 2026
Revised: 20 March 2026
Accepted: 25 March 2026
Published: 27 March 2026

exposure and vulnerability within the ESRM20 framework [2]. A common strategy for modeling material strength in nonlinear computational analyses is the adoption of mean strength values to represent the expected mechanical behavior. This approach has been applied for the seismic vulnerability assessment of both new and existing structures, as well. Given the increasing adoption of advanced nonlinear modeling techniques, including detailed finite-element and fiber-based approaches, the necessity for reliable constitutive models and material parameters has grown substantially. These models rely on accurate stress–strain relationships to capture essential nonlinear behaviors such as cracking, yielding, bar buckling, and confinement effects, which are central to predicting failure mechanisms under strong ground motions. The study of Xiao et al. [3] investigates the influence of carbonation on the compressive behavior of concrete by testing twenty-seven prisms under monotonic uniaxial loading, showing that carbonation increases compressive strength while significantly reducing deformation capacity. Complementary tests on reinforced concrete beams and columns demonstrate that carbonation adversely affects global structural performance, ultimately reducing the earthquake resistance of RC elements. The study of Diamantopoulos et al. [4] investigates the seismic fragility and risk of reinforced concrete structures subjected to aging caused by chloride-induced corrosion, identifying the key parameters influencing corrosion initiation and its impact on seismic performance. A risk-targeted methodology is proposed to determine minimum cover depths that ensure an acceptable target risk, validated through the analyses performed on a four-storey RC building designed to modern code provisions. The research of Kordtabar et al. [5] quantifies the time-dependent impact of chloride-induced corrosion on the seismic and serviceability reliability of an RC frame by integrating a corrosion progression model with nonlinear finite-element analysis and FORM. Results show that corrosion markedly increases failure probabilities for both seismic damage states and serviceability limits over a 60-year life span, with initiation time, diffusion coefficient, and rebar diameter emerging as the dominant uncertainty parameters. In reference [6], a carbonation-induced corrosion model is integrated into a seismic fragility framework to quantify how environmental factors such as CO_2 concentration, humidity, and temperature degrade the seismic performance of RC buildings in inland urban environments over time. Results indicate a progressive increase in damage probabilities and a shrinking safety margin between severe damage and collapse after the design durability life, highlighting the need to explicitly account for time-dependent deterioration in seismic assessments of aging RC structures. The study of Shi et al. [7] evaluates the time-dependent seismic fragility of an offshore bridge by incorporating both carbonation and chloride-induced corrosion into a degradation-aware structural model and performing incremental dynamic analysis on its components and system. Results show that fragility increases markedly over the service life, with the bridge system consistently more vulnerable than individual components. The paper of Nigro et al. [8] presents a practice-oriented procedure for assessing the seismic reliability of existing RC buildings by incorporating carbonation-induced material degradation and using nonlinear static (pushover) analyses as an efficient alternative to nonlinear time-history simulations. A case study demonstrates how key parameters, particularly exposure class and concrete cover, significantly influence the time-dependent seismic reliability of aging RC buildings constructed prior to modern seismic design principles. In reference [9], an investigation on how carbonation-induced corrosion, driven by elevated CO_2 concentrations in urban and industrial environments, progressively reduces the seismic capacity and increases the collapse probability of a modern RC moment frame over a 50-year service life is shown. Using nonlinear static and incremental dynamic analyses at 5-year intervals, the results show significant time-dependent degradation in both load-bearing performance and seismic fragility under different environmental exposure scenarios. The paper of

Zheng et al. [10] proposes a probabilistic framework for time-variant seismic fragility of high-rise buildings subjected to carbonation-induced corrosion, incorporating Bayesian updating, analytical corrosion-initiation modeling, and copula-based dependence between limit states. Application to a 42-storey SFRCT building shows that uncertainties in corrosion initiation markedly increase seismic demand and fragility, while Gaussian and Clayton copulas yield similar joint fragilities, with the Clayton copula offering broader applicability. The paper of Sung and Su [11] evaluates how carbonation-induced neutralization degrades the seismic capacity of RC bridge columns by deriving time-dependent plastic-hinge properties, performing pushover analyses, and generating fragility curves and seismic loss functions over the service life. S-surfaces relating retrofit cost to service time and earthquake intensity reveal critical points where costs escalate sharply, enabling optimization of timely seismic retrofitting strategies. The study of Samanta et al. [12] assesses the seismic risk of Indian RC wall–frame buildings with low wall density by incorporating both aging-induced corrosion and sequential ground motions into a performance-based analytical framework, producing fragility, vulnerability, and annual seismic damage rates for different corrosion scenarios. Results show that the combined deterioration and repeated shaking substantially amplify near-collapse risk and financial losses, while the proposed method quantifies insurance parameters and highlights the importance of including aging and sequential GM effects in risk-informed mitigation and insurance decisions.

Most existing frameworks rely on idealized material properties or Western European concrete carbonation constants that do not account for the specific chemical compositions of Romanian cements used between 1950 and 2000. Furthermore, while previous studies for Bucharest have utilized simplified fragility curves, they largely overlook the stochastic nature of the reinforcing steel types and the resulting impact on structural overstrength. This lack of a localized, statistically based material model constitutes a significant gap in the current risk assessment of the region. To address this, the objective of this study is to examine how construction-era variability in material properties influences the seismic vulnerability of reinforced concrete buildings in Bucharest. Regional vulnerability assessments often rely on simplified assumptions regarding material strengths, deterioration, and structural behavior due to limited historical data and case-study evidence. This work addresses these limitations by statistically characterizing historical reinforcing steels and concretes used in the period 1950–2000 and developing probabilistic models for their mechanical properties. While the probabilistic models developed in this study leverage the most extensive archival datasets available for Bucharest, it is acknowledged that these historical records may not fully encompass the inherent spatial variability or site-specific quality inconsistencies across the city's entire building stock. These models are then incorporated into the nonlinear analysis of a representative pre-1970 RC building to assess how era-specific strength, ductility, and overstrength affect structural capacity and fragility. The study also integrates carbonation-induced reinforcement corrosion into the seismic assessment framework to quantify how time-dependent deterioration modifies capacity curves, fragility functions, and seismic losses. Through this combined material- and structural-level approach, the research provides a more realistic basis for evaluating the seismic vulnerability and long-term risk of Bucharest's aging RC building stock.

2. Statistical Characterization of Historical RC Materials

In this section, probabilistic models are formulated to represent material strengths and deformation capacities through statistical distributions derived from experimental datasets and historical records. A brief description of the evolution of construction materials employed in the period 1940–1990 for the RC structures constructed in Bucharest can be found in the recent book of Pavel and Ioan [13]. Additional relevant information for this study can be found in a book by Avram [14], as well as in a book by Carare [15]. Some construction details for various RC elements can be found in a paper by Pavel et al. [16].

Prior to the implementation of Eurocode 2-compliant reinforcement standards [17], three principal categories of steel reinforcement (OL38 or OB37, TOR47 and PC52) were predominantly utilized in reinforced concrete structures throughout Romania. Among the three types of reinforcement, the first one was smooth, and the last two were ribbed. The PC52 steel was introduced in the early '60s, while the TOR47 was used until the late '60s [15]. OB37 and PC52 were obtained through a hot-rolling process, while TOR47 was fabricated via cold twisting around the bar axis of hot-rolled round profiles manufactured from OL 38 grade steel at the beginning, which was also used for OB37 reinforcement (or OL 42 in the subsequent periods). The impact of this procedure on the resulting reinforcement was an increase of 45–60% of the yield strength, an increase of about 15% of the ultimate strength and a 40–50% decrease in the ultimate strain [15]. The use of TOR47 was discontinued owing to a series of deficiencies related to their weldability, the lack of homogeneity in the rib pitch, or their poor fatigue behavior.

The design strengths of these reinforcing steel types are summarized in Table 1 based on the design codes for reinforced concrete structures enforced in the period 1950–2000.

Table 1. Nominal design yield strengths of reinforcing steel types according to historical Romanian design codes (1950–2000).

Reinforcement Type	**Design Strength (N/mm^2)**			
	STAS 1546-50 [18]	**P8-62 [19]**	**STAS 10107/0-76 [20]**	**STAS 10107/0-90 [21]**
OB37	285	210	210	210
TOR47	-	280	-	-
PC52	-	290	290	300

Additional relevant information for the three types of reinforcing steel in terms of minimum yield strengths, ultimate strengths and ultimate strains is reported in Table 2, based on the values provided in three codes valid in the 1950–1990 period.

Table 2. Prescribed mechanical properties for historical reinforcing steel grade [22–24].

Reinforcement Type	**Code**								
	STAS 438-54 [22]			**STAS 438-61 [23]**			**STAS 438/1-80 [24]**		
	$f_{y,min}$ (N/mm^2)	**$f_{u,min}$ (N/mm^2)**	**$\varepsilon_{su,min}$ (%)**	**$f_{y,min}$ (N/mm^2)**	**$f_{u,min}$ (N/mm^2)**	**$\varepsilon_{su,min}$ (%)**	**$f_{y,min}$ (N/mm^2)**	**$f_{u,min}$ (N/mm^2)**	**$\varepsilon_{su,min}$ (%)**
OB37	220	380	21	240	380	21	235/255 (as a function of diameter)	360	25
TOR47	-	-	-	380	470	10	-	-	-
PC52	-	-	-	370	520	18	335/355 (as a function of diameter)	510	20

$f_{y,min}$: minimum yield strength; $f_{u,min}$: minimum ultimate strength; $\varepsilon_{su,min}$: minimum ultimate strain.

An important factor that consistently influences the load-carrying capacity of reinforced concrete (RC) elements is the actual strength of the reinforcing steel. Based on an examination of data reported in multiple studies addressing the temporal variation in reinforcement strength, the synthesized findings are presented in Figure 1 and Table 3 [25]. Figure 1 illustrates the relative-frequency distributions of both the yield strength and the ultimate strength for the three investigated steel types: OB37, TOR47 and PC52.

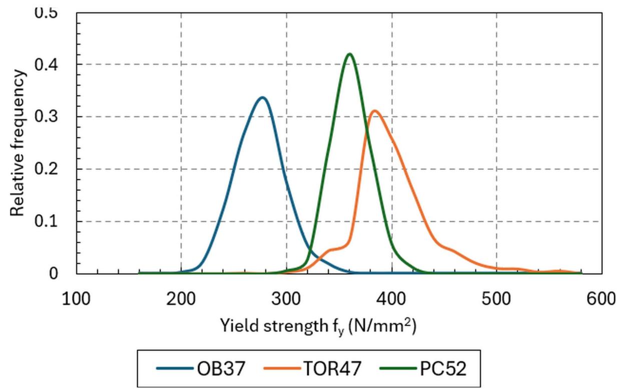

(a)

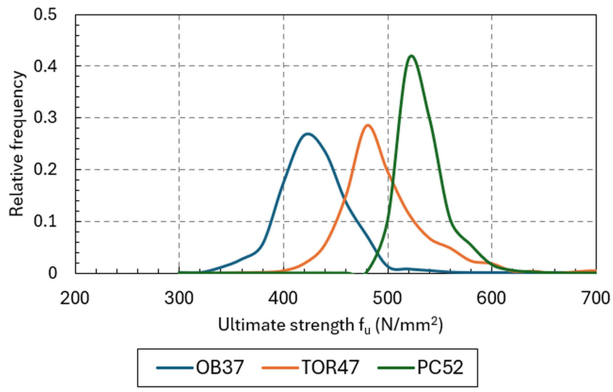

(b)

Figure 1. Relative frequency histograms for: (**a**) reinforcement yield strength, f_y [25]; (**b**) reinforcement ultimate strength, f_u [25].

Table 3. Statistical parameters for strength ratios and normalized mean strengths of historical reinforcement.

Reinforcement Type	Parameter				
	(f_u/f_y)—Median	**(f_u/f_y)—5th Percentile**	**(f_u/f_y)—95th Percentile**	$\mathbf{f_{y,mean}/f_{yd}}$	$\mathbf{f_{u,mean}/f_{yd}}$
OB37	1.56	1.44	1.68	1.31	2.04
TOR47	1.24	1.01	1.51	1.43	1.77
PC52	1.48	1.32	1.66	1.20	1.78

f_{yd}: design yield strength; $f_{y,mean}$ and $f_{u,mean}$ represent mean yield and ultimate strengths, respectively.

The histograms indicate clear differences in the mechanical performance of the steel classes. OB37 exhibits the lowest yield-strength values, predominantly ranging between approximately 220–320 N/mm^2, while TOR47 shows a higher and comparatively narrower distribution centered around 350 N/mm^2. In contrast, PC52 demonstrates the highest yield-strength levels, with peak frequencies occurring near 380–420 N/mm^2, suggesting a more consistent production quality. A similar trend is evident for ultimate strength: OB37 again occupies the lowest strength range (roughly 380–500 N/mm^2), TOR47 displays intermediate values clustered around 480–520 N/mm^2, and PC52 reaches the highest levels, with a pronounced peak near 520–580 N/mm^2.

Overall, the results confirm a progressive increase in both yield and ultimate strength from OB37 to TOR47 to PC52. The relatively narrow distributions observed for PC52 further indicate reduced variability, which is beneficial for structural reliability.

Additional parameters that can be evaluated using the available experimental data include the ratio between the ultimate strength and the yield strength of the reinforcing steel, as well as the ratio between the mean and the design strength. The former ratio constitutes a key mechanical indicator in the seismic design of reinforced concrete structures, as it directly reflects the material's capacity to sustain inelastic deformations and thus governs the ductility and energy-dissipation potential of structural members. To quantify these effects, the relevant statistical parameters were computed assuming a lognormal probability distribution for both the yield and the ultimate strength. A correlation coefficient of 0.85 between the ultimate and the yield strength was considered according to the JCSS Model Code [26]. The resulting values are synthesized in Table 3, summarizing the median, 5th percentile and 95th percentile ratios between ultimate strength and yield strength (f_u/f_y), as well as the ratio between the mean yield ($f_{y,mean}$) and ultimate strengths ($f_{u,mean}$) normalized and the design strength (f_{yd}).

According to Eurocode 2 [17], Type C ductile reinforcement, which is required in seismic design, must satisfy a f_u/f_y ratio between 1.15 and 1.35, and the ratio between the mean and design yield strengths is typically taken as 1.32. When compared with these reference values, the steels in the table exhibit noticeably different behaviors. OB37 and PC52 show substantially higher f_u/f_y ratios (median values of 1.56 and 1.48, respectively), indicating a much larger available ductility and strain-hardening capacity than the upper limit prescribed by Eurocode 2. TOR47, on the other hand, has a median f_u/f_y ratio of 1.24, which falls within the Eurocode 2 envelope, although with greater variability (1.01–1.51). Regarding the overstrength, the values of $f_{y,mean}/f_{yd}$ in the table (1.20–1.43) show that TOR47 exceeds the Eurocode-based reference value (~1.32), OB37 is close to it, and PC52 lies slightly below. This confirms that the three historical steel types exhibit different combinations of ductility and overstrength, with OB37 being highly ductile, TOR47 being strong but with limited ductility, and PC52 occupying an intermediate position. The values in the table show significantly higher overstrengths for all three historical steel types when compared to this reference. OB37 reaches the highest value ($f_{u,mean}/f_{yd}$ = 2.04), indicating that its real failure strength is more than double the design yield strength. PC52 also shows a large reserve (1.78) as well, while TOR47 exhibits a similar magnitude (1.77), despite its lower ductility. This highlights an important distinction: although TOR47 has a relatively low f_u/f_y ratio, meaning limited post-yield ductility, its absolute failure strength is nonetheless much higher than the code-level design strength. In contrast, OB37 combines very high ductility with very high ultimate overstrength, making it particularly robust in terms of deformation capacity and reserve strength. PC52 remains intermediate in both aspects.

The evaluation of concrete quality differed substantially between the period before 1990 and the period after 1990, reflecting both the statistical treatment of strength data and the control procedures applied on site. When concrete was classified based on the mean compressive strength of 20 cm cubes (before 1990), quality control relied primarily on verifying that the average of a limited number of tests met or exceeded the nominal class strength. This approach provided only a partial measure of structural reliability, as the mean strength alone does not characterize the variability of production, nor does it ensure that a sufficient proportion of specimens meets the design requirements. After 1990, with the adoption of classification based on the characteristic strength corresponding to the 5th percentile computed using the normal distribution, concrete quality could be assessed in a more statistically consistent manner. By explicitly accounting for the expected variance of the results, the characteristic value enabled an evaluation of both central tendency and variability and thus provided a more robust indicator of the probability that in situ concrete meets design performance. This shift also aligned quality control with modern limit-state design principles, where reliability is explicitly quantified through probabilistic models of material resistance.

Another aspect that must be considered is the progressive increase in the compressive strength of concrete used in residential construction during the second half of the twentieth century. Throughout the period leading up to 1990, typical concrete grades for mass-housing and standard residential buildings gradually evolved from C12/15 equivalent mixes toward strengths approaching C20/25, reflecting improvements in material technology, mix design, and production control [14]. This transition was driven not only by updated material specifications in successive standards, but also by the increasing structural demands associated with higher building stock densities, the widespread adoption of large-panel prefabrication systems, and the need for improved performance under seismic loading. From a quality-assessment perspective, this gradual shift in nominal strength classes indicates a systematic enhancement of both material consistency and reliability. Higher-strength concretes typically exhibit lower coefficients of variation, improved durability, and better performance under cyclic and dynamic actions. The decrease in the coefficients of variation with the concrete class increase is also adopted in modern design codes (e.g., Eurocode 2 [17]). Consequently, the upward trend in concrete strength, together with the post-1990 adoption of the characteristic (5th percentile) strength as the basis of classification, contributed to a more robust and statistically coherent framework for evaluating the in-situ quality of concrete and ensuring compliance with reliability-based design principles.

The statistical analysis of the concrete compressive strength is also relevant for a thorough understanding of the seismic fragility of RC structures. A comparison between the mean concrete strengths, the corresponding coefficients of variation and the 5th percentile computed using the normal probability distribution, as a function of the prescribed class for concrete cast on-site and for factory-produced concrete for the 1968–1983 period, is shown in Table 4 [27]. The compressive strength values in Table 4 refer to values obtained from 200 mm cubes. The results from Table 4 reveal that the in situ concrete strength distributions frequently fell below the 5th percentile requirements, signaling a non-compliance with the prescribed concrete classes. The coefficient of variation was in almost all cases lower than the 15% limit specified in the design codes for reinforced concrete structures.

Table 4. Statistical comparison of compressive strength for site-cast and factory-produced concrete (1968–1983) [27].

Concrete Class	Concrete Cast In-Situ			Factory-Produced Concrete		
	Mean	Coefficient of Variation	5th Percentile	Mean	Coefficient of Variation	5th Percentile
C20/25	24	13.2	18.8	30.6	19.5	20.8
C25/30	25.5	13	20.1	33.8	16.7	24.5
C30/37	-	-	-	42.5	12.1	34.0

All values are expressed in N/mm^2. The 5th percentile values are calculated based on a normal distribution.

Concrete cover thickness constitutes another critical parameter governing the cyclic response of reinforced concrete elements, as inadequate cover can precipitate premature buckling of longitudinal reinforcement once lateral confinement is lost. In addition, insufficient cover accelerates deterioration processes such as corrosion, thereby compromising both the deformation capacity under seismic loading and the long-term durability of the structural system.

Table 5 reports the minimum concrete cover thicknesses for beams and columns in reinforced concrete (RC) structures, as prescribed by the design codes applicable during the period spanning 1950 to 2000.

Table 5. Prescribed minimum concrete cover thicknesses for RC beams and columns (1950–2000).

Structural Element	Design Strength (N/mm^2)			
	STAS 1546-50 [18]	P8-62 [28]	STAS 10107/0-76 [20]	STAS 10107/0-90 [21]
Beam	25 mm	25 mm	25 mm	20–35 mm (as a function of the exposure conditions)
Column	25 mm	25 mm	25 mm	20–35 mm (as a function of the exposure conditions)

3. Benchmark Case Study

The probabilistic characterization of historical reinforcing steels and concretes provides the foundation for developing realistic nonlinear models of existing RC buildings. However, the material-level analysis is only the first component of the study. To examine how these construction-era material properties influence structural response, a pre-1970 RC building is analyzed separately. This RC building has typical reinforced concrete element detailing, which reflects common practices of that era, making it suitable as a representative example. The following section introduces the case-study structure, which is evaluated independently from the material characterization in Section 2.

The analyzed building is an 11-storey RC structure designed and built before 1970. The case study is a dedicated office building with a purely open-plan configuration surrounding a central RC core. The design of the building was performed considering the P13-63 code [29]. The structural layout consists of a central core having a thickness of 30 cm at the ground storey and 25 cm for the upper stories and RC frames. The beams have a 30 × 80 cm cross-section, while the columns have a rectangular cross-section of 40 × 70 cm. The boundary elements of the structural walls have a 50 × 50 cm cross-section. The structure has a height of 41.14 m, with the height of all the stories being 3.74 m. The structural layout is illustrated in Figure 2, with the dimensions provided in meters. The building utilizes the exact material classes (OB37 plain reinforcing steel and B250 concrete) characterized in the first part of this study, ensuring that the structural analysis is grounded in the historical reality of Romanian construction practice. A fixed-base condition was assumed to isolate the impact of material variability on structural fragility. While Bucharest's soft soils can influence response through Soil–Structure Interaction (SSI), the high stiffness of the core wall system and the long-period characteristics of Vrancea earthquakes suggest that a fixed-base model provides a stable and conservative baseline for evaluating the seismic performance.

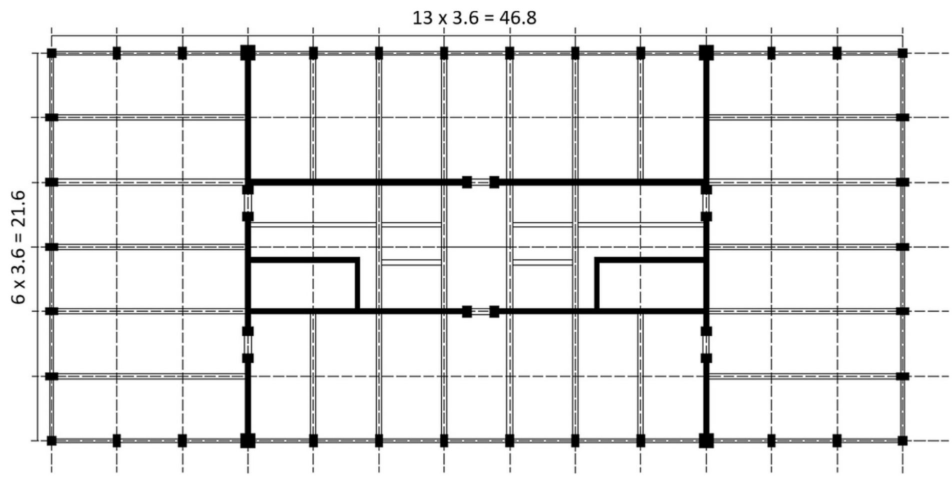

Figure 2. Structural layout of the analyzed building.

The dynamic properties of the model (eigenperiods and corresponding participation mass ratios) are given in Table 6. The values shown in Table 6 are obtained using mean material strengths.

Table 6. Dynamic properties and mass participation ratios of the 11-storey structural model.

Mode nr.	T (sec.)	Mass Participation Ratios (%)		
		Translation–Longitudinal	Translation–Transversal	Torsion
1	0.50	0.0	69.3	2.6
2	0.46	0.0	2.4	76.9
3	0.30	71.7	0.0	0.0
4	0.15	0.0	1.7	10.1
5	0.14	0.0	15.2	0.9
6	0.10	8.6	0.0	0.0

The structure was moderately affected by the Vrancea intermediate-depth earthquake of 4 March 1977 (moment magnitude M_W = 7.4 and focal depth of 94 km). Damage was observed in the coupling beams, the floor slabs, and the boundary elements of the core wall system [30]. The damage to the boundary elements was concentrated in the bottom four stories, while the coupling beams and slab damage occurred up to the eighth storey. An important aspect that was evaluated through non-destructive testing after the earthquake was the concrete compressive strength in the core walls. The results are reported in Table 7. The design concrete class was similar to C16/20, with a mean strength of 25 N/mm^2. It can be easily observed from Table 7 that the real concrete strength was significantly lower than the design one, especially for the bottom stories. In the upper stories, some localized values approached or exceeded the design mean. However, there is a much larger scatter in the concrete compressive strengths in the upper stories. This observation is in line with the results shown in Table 3 regarding the non-compliance of cast-in-situ concretes with the prescribed classes. It is important to note that for the seismic assessment of the case-study structure, the concrete strength parameters are not derived from the general probabilistic framework of the building stock discussed previously. Instead, they are based on direct in situ measurements obtained from post-earthquake testing, which revealed actual compressive strengths significantly lower than the original design values, thereby ensuring the model reflects the true condition of the building.

Table 7. Measured variation in concrete compressive strength across storey levels for the case-study structure [30].

Storey	Concrete Compressive Strength Range (N/mm^2)
Ground	15–20
1	18–20
2	16–20
3	14–17
4	21–23
5	25–28
6	23–24
7	18–26
8	18–20
9	17–29
10	19–28

Data derived from post-1977 earthquake non-destructive testing.

In order to validate the findings from the nonlinear static analysis, an evaluation of the capacity of the structural walls is performed using the empirical relations proposed by Abdullah and Wallace [31] and Pavel et al. [32] for the evaluation of the displacement capacity—Equations (1) and (2)—and that proposed by Wood [33] for the susceptibility of the longitudinal reinforcement fracture—Equation (3).

$$\theta_{cap} = 3.85 - \frac{\lambda_b}{\alpha} - \frac{\nu_{max}}{0.83 \cdot \sqrt{f_{ck}}} \tag{1}$$

$$log\theta_{cap} = -1.537 - 1.719 \cdot ALR - 0.026\frac{H_w}{l_w} - 0.023\frac{l_w}{b} + 5.08 \cdot \rho_{wh} + 35.14 \cdot \rho_{bh} \tag{2}$$

In Equation (1), $\lambda_b = l_w \cdot c/b^2$, where l_w is the length of the cross-section, c is the neutral axis depth, b is the thickness of the compression zone of the wall, and α is 60, where overlapping hoops are used, and 45, where a combination of a single perimeter hoop with supplemental crossties is used. $\nu_{max}/\sqrt{f_{ck}}$ represents the shear stress ratio.

In Equation (2), ALR is the axial load ratio, H_W is the structural wall height, ρ_{wh} is the web horizontal reinforcement ratio, and ρ_{bh} is the boundary element horizontal reinforcement ratio.

$$I = \frac{\left(\rho_t \cdot f_y + \frac{N}{A_c}\right)}{f_{ck}} \tag{3}$$

In the equation above, ρ_t represents the total longitudinal reinforcement ratio, f_y is the reinforcement yield strength, N is the axial force, and A_c denotes the cross-sectional area of the reinforced concrete structural wall. Values of this indicator below 0.15 suggest that the RC wall is susceptible to this phenomenon under cyclic loading.

The resulting displacement capacities and of the indicator I, for one longitudinal and one transversal structural wall, are reported in Table 8. It can be observed from Table 8 that the two structural walls are not susceptible to longitudinal reinforcement rupture. Noticeable differences between the empirical drift capacities can be observed, as well.

Table 8. Calculated displacement capacities (θ_{cap}) and performance indicator I for selected structural walls.

Direction	θ_{cap} [31]	θ_{cap} [32]	I [33]
Long.	0.77%	0.47%	0.19
Transv.	1.22%	0.71%	0.22

4. Seismic Capacity and Fragility Assessment of the Case-Study Building

The seismic capacity of the structure is derived via static nonlinear analysis. The analyses are performed in SeismoStruct software version 2024 [34]. The concrete and reinforcement are modeled using the Mander et al. [35] hysteretic model and the Menegotto–Pinto model [36], respectively. The resulting capacity curves for the two principal directions, together with their corresponding bilinear idealizations, are presented in Figure 3. The bilinear idealization of the capacity curves was performed in accordance with the equal energy rule. The stiffness of the linear curve was defined as the secant stiffness at 60% of the ultimate base shear capacity.

In Figure 3a, the capacity curve in the longitudinal direction displays a higher strength, reaching spectral accelerations close to 0.47–0.50 g before stabilizing into the plastic range. As shown in Figure 3b, the transversal direction exhibits a gradual increase in strength up to a peak spectral acceleration of approximately 0.34 g, followed by a slight post-peak softening. The bilinear approximations closely match the initial stiffness and the plateau region of the curve. These bilinear curves are later used to derive the equivalent single-degree-of-freedom parameters required for subsequent seismic performance assessment.

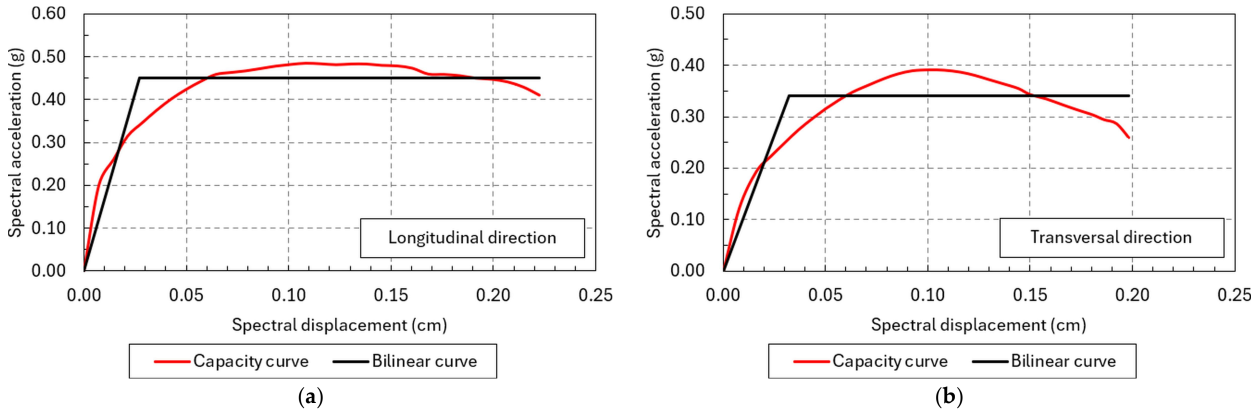

Figure 3. Pushover curves and corresponding bilinear curves for the case-study structure: (**a**) longitudinal direction; (**b**) transversal direction.

The fragility functions for the analyzed structure are obtained using an approach based on the Incremental Dynamic Analysis (IDA) [37] and an equivalent single degree of freedom (SDOF) system. A ground motion dataset consistent with the seismic hazard of Bucharest, consisting of 20 ground motions recorded in the Bucharest area during the major Vrancea intermediate-depth earthquakes of 1977, 1986 and 1990, is employed. The dataset has been previously employed in other studies with the same focus (e.g., [38,39]). The Incremental Dynamic Analysis used the peak ground acceleration as the scaling intensity measure, aligning the structural assessment with the seismic hazard definition for Bucharest. Scaling based on PGA preserves the relative spectral shape of the selected Vrancea ground motions, which is particularly important for high-rise core wall structures where higher-mode effects and period elongation are significant factors.

The parameters (median-θ and logarithmic standard deviation-β) of the lognormal fragility functions are summarized in Table 9. The displacement thresholds corresponding to each damage state were considered based on the approach from the European Seismic Risk Model (ESRM20) [40]. The fragility assessment employs a mean structural model to represent the typical building response, while uncertainties are accounted for through the total logarithmic standard deviation. The aleatory uncertainty, representing record-to-record variability, is derived from the dispersion of the IDA results. The epistemic uncertainty associated with the historical material properties is incorporated analytically into the total dispersion using the SRSS (Square Root of the Sum of Squares) method.

Table 9. Median (θ) and dispersion (β) parameters for the seismic fragility functions of the case-study building.

Direction	Damage State							
	Slight Damage		Moderate Damage		Extensive Damage		Complete Damage	
	θ (g)	β	θ (g)	β	θ (g)	β	θ (g)	β
Long.	0.17	0.44	0.24	0.52	0.39	0.67	0.71	0.77
Transv.	0.16	0.43	0.22	0.52	0.34	0.69	0.62	0.84

The fragility functions for the two principal directions are plotted in Figure 4, illustrating the probability of exceeding each damage state as a function of PGA and highlighting the higher vulnerability in the transversal direction for the more severe damage states.

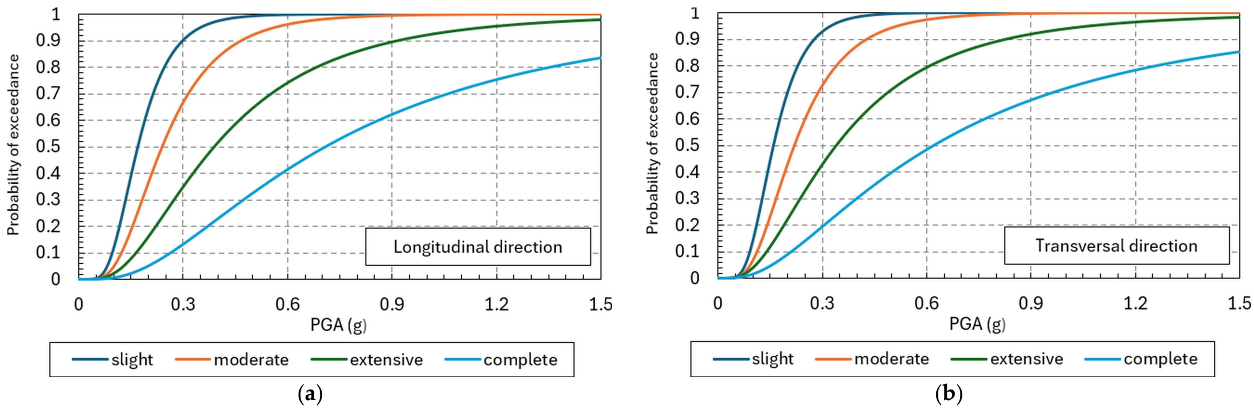

Figure 4. Fragility functions for the case-study structure: (**a**) longitudinal direction; (**b**) transversal direction.

5. Time-Dependent Deterioration and Its Effects on Seismic Fragility and Risk

Carbonation-induced reinforcement corrosion significantly increases the seismic fragility of reinforced concrete structures by degrading material properties over time. Carbonation reduces the alkalinity of concrete, initiating corrosion in steel reinforcement, which leads to reduced cross-sectional area, loss of ductility, and weakened bond strength between steel and concrete. In reference [41], it is mentioned that a significant reduction in the elongation at maximum load of 30% and 50% was found for cross-section losses of 15 and 28%, respectively. However, corrosion that causes a more uniform mass loss along the bar length (as is the case of carbonation-induced corrosion) has little influence on the mean tensile stress–strain response, since the mean stress is calculated using the uniformly reduced diameter [42]. In this study, reinforcement degradation is modeled as uniform (general) corrosion, which is the primary morphological outcome of carbonation-induced deterioration. While localized pitting corrosion can lead to more significant reductions in bar cross-sections and premature brittle fracture, it is predominantly associated with chloride-induced corrosion, a mechanism typically found in coastal regions or areas with heavy de-icing salt usage. Given that Bucharest is characterized by an inland environment with negligible chloride exposure, carbonation is the dominant driver of long-term atmospheric corrosion for the existing RC building stock. Therefore, the uniform corrosion assumption is considered a representative approximation for assessing the time-dependent loss of lateral capacity and stiffness.

The equations proposed in [42] for the yield-f_{yt} and ultimate stresses-f_{ut} of corroded bar based on the original cross section area are as follows:

$$f_{yt} = f_y \cdot (1 - 0.017\psi) \quad (4)$$

$$f_{ut} = f_y \cdot (1 - 0.018\psi) \quad (5)$$

where ψ is the mass loss in percentage and f_y and f_u are the yield and ultimate stresses of the uncorroded bar.

The computations for the evaluation of the carbonation-induced corrosion were performed using various documents in the literature (e.g., [43,44]). The carbonation depth at time t can be estimated using the following equation:

$$x_c(t) = k \cdot t^b \quad (6)$$

In the above relation, k represents the apparent natural carbonation rate, t is the time and b = 0.5. Values for the parameter k can be found in the literature for various cement types and water/cement ratios.

A full probabilistic design approach for the modeling of carbonation depth at time t is given in [44] or [45] as:

$$x_c(t) = \sqrt{2 \cdot k_e \cdot k_c \cdot R_{NAC,0}^{-1} \cdot C_s} \cdot \sqrt{t} \cdot W(t) \tag{7}$$

where k_e is an environmental function, k_c is an execution transfer parameter, C_s is the CO^2 concentration in the air, W(t) is a weather function, and $R_{NAC,0}^{-1}$ is the inverse effective carbonation resistance of concrete and is evaluated using the following relation ([44,45]):

$$R_{NAC,0}^{-1} = k_t \cdot R_{ACC,0}^{-1} + \epsilon_t \tag{8}$$

where $R_{ACC,0}^{-1}$ inverse effective carbonation resistance of dry concrete, determined at a certain time t_0 using the accelerated carbonation test, k_t is a regression parameter for the test effect of the ACC (Accelerated Carbonation Coefficient) test, and ε_t is an error term for inaccuracies that occur conditionally when using the ACC test method.

The reduction in the diameter of the reinforcement bar due to corrosion is [46]:

$$D(t) = D_i - i_{corr} \cdot (t - T_{init}) \tag{9}$$

where D_i is the initial diameter of the rebar, and i_{corr} is the corrosion rate.

The study of Dhakal and Maekawa [47] shows that two main mechanisms lead to splitting cracks and, eventually, to the spalling of the concrete cover. First, high compressive strains damage the cover concrete and create vertical cracks, which reduce its ability to resist tension. Then, as the longitudinal bar begins to buckle, these cracks widen further until the cover concrete can no longer provide any tensile resistance and separates from the core concrete. Analytical models have been developed in the literature (e.g., [48,49]) to simulate the cyclic behavior of reinforcing steel, many of which explicitly incorporate the effects of inelastic buckling on strength degradation, stiffness deterioration, and overall hysteretic response. The study of Yang et al. [50] experimentally investigates the inelastic buckling behavior of longitudinal reinforcing bars in reinforced concrete columns under seismic conditions. The parameter λ_p, proposed by Dhakal and Maekawa [47] to check if premature buckling of the reinforcement occurs, is:

$$\lambda_p = \frac{L}{D} \cdot \sqrt{\frac{f_y}{100}} \tag{10}$$

where L is the buckling length of the longitudinal reinforcing bar, and D is its diameter. If the value of λ_p is less than or equal to eight, premature buckling can be avoided.

The reduced concrete cover compressive strength f_c* can be evaluated using the model developed in [51]:

$$f_c^* = \frac{f_c}{1 + K\frac{\varepsilon_1}{\varepsilon_{c0}}} \tag{11}$$

where K is a coefficient related to bar roughness and diameter, ε_1 is the average tensile strain of the cracked concrete, and ε_{c0} is the strain at peak compressive stress. ε_1 can be evaluated with the following relation [51]:

$$\varepsilon_1 = \frac{b_f - b_0}{b_0} \tag{12}$$

where b_0 is the initial section width before the corrosion initiation, and b_f is the increased section width due to rust expansion and corrosion cracking. An approximation for $b_f - b_0$ is as follows [51]:

$$b_f - b_0 = no._{bars} \cdot w_{cr} \tag{13}$$

where $no._{bars}$ is the number of rebars under compression, and w_{cr} is the total crack width for a given corrosion level, which can be computed with the equation [51]:

$$w_{cr} = 2\pi(\nu_{rs} - 1)X \tag{14}$$

where ν_{rs} is the ratio of the volumetric expansion of the rust products with respect to the initial material (taken as equal to 2), and X is the depth of the corrosion attack.

A simple evaluation of the carbonation depth, considering a time interval of 50 years and using experimental data shown in [52] in Equation (6), shows that the depth is about 15 mm for an interior environment with relative humidity (RH) above 70% and 28 mm for an interior environment with relative humidity less than 50%. Consequently, in the latter case, the carbonation depth exceeded the concrete cover of 25 mm. The apparent natural carbonation rate is defined as mm/$\sqrt{}$year with a standard deviation of mm/$\sqrt{}$year. The values of the apparent natural carbonation rate are adopted from the experimental characterization of CEM I through CEM III cements, the primary binders used in the case-study era, as established in the specialized research of Moraru [53]. These values correspond to an XC3 exposure class (moderate humidity) and a mean annual relative humidity of approximately 65–70%, which are consistent with the multi-decadal climatic averages of Bucharest. This statistical distribution allows for a probabilistic representation of the carbonation depth over the structural lifespan. By applying a First Order Reliability Model (FORM) [54] and considering the concrete cover of 25 mm and a standard deviation of 10 mm, as well as the parameters mentioned above for K, the exceedance probabilities in 10, 20 and 50 years are of 17%, 36% and 61%, respectively. This shows that within the service life of the structure, it is very likely that the carbonation depth exceeds the concrete cover. The initiation time for the carbonation-induced corrosion is of about 39 years. This means that, currently, the building has been subjected to such a phenomenon for about 17 years. The reduction in the diameter of the reinforcement bar due to corrosion, considering a corrosion rate of 1 $\mu A/cm^2$, is about 0.2 mm. Thus, the reduction in terms of area for 20 mm reinforcing bars, which were employed for the longitudinal reinforcement, is about 1%, while for the 8 mm bars employed for the transversal reinforcement, the reduction is about 5%. Based on these values, it can be concluded that for the analyzed building, the yield and ultimate steel strength remain unchanged. The elongation at maximum load is reduced by 16% for the 8 mm bars and by 10% for the 20 mm bars. The structural impact of reinforcement corrosion is incorporated into the non-linear model by reducing the cross-sectional area of the longitudinal and transversal reinforcement. This approach prioritizes the loss of steel area as the primary driver of capacity degradation. Finally, the resulting pushover curves and fragility functions for the case-study structure affected by corrosion are shown in Figures 5 and 6. Considering the actual spacing of the stirrups in the boundary elements of the case-study structure (150 mm or 200 mm) and the diameter of the longitudinal bars, premature buckling failure can be expected as the value of the indicator λ_p is well above the limit value of 8.

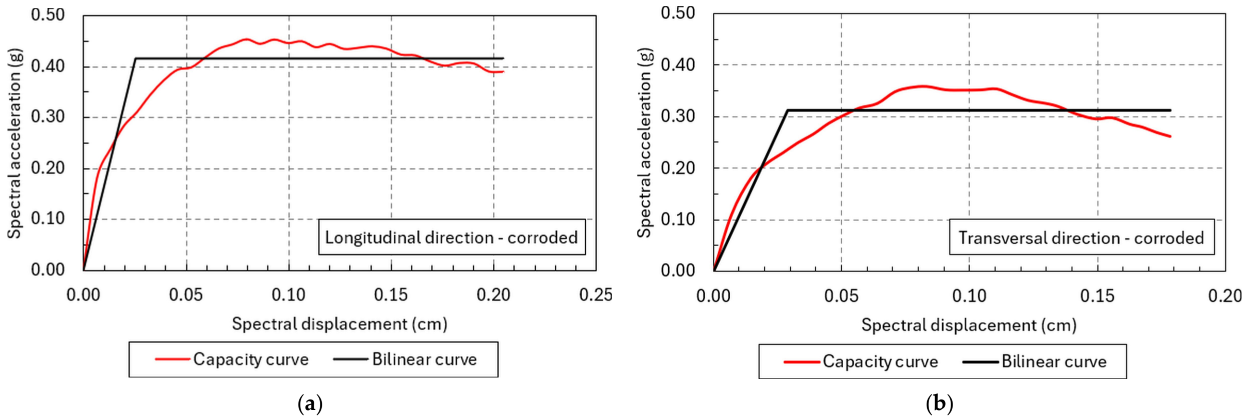

Figure 5. Pushover curves and corresponding bilinear curves for the case-study structure affected by corrosion: (**a**) longitudinal direction; (**b**) transversal direction.

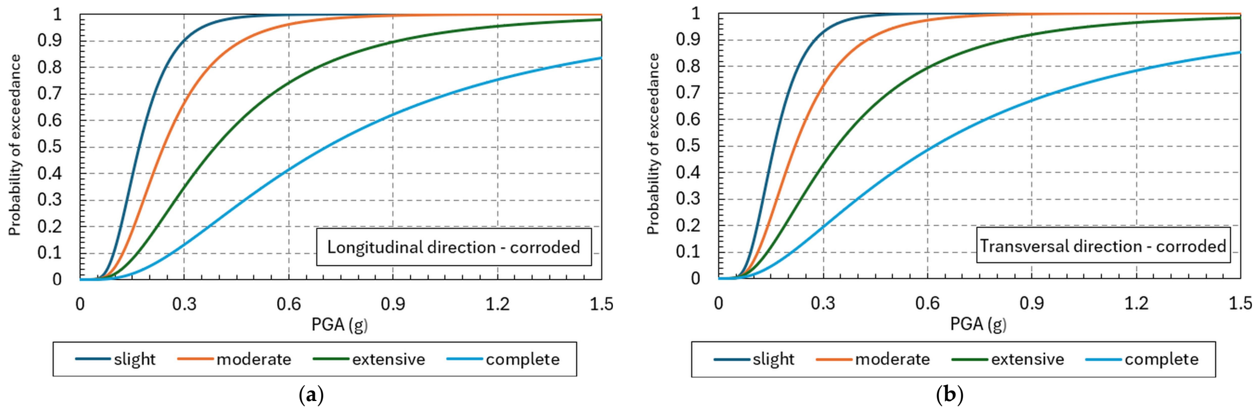

Figure 6. Fragility functions for the case-study structure affected by corrosion: (**a**) longitudinal direction; (**b**) transversal direction.

Figure 5 illustrates the effect of carbonation-induced reinforcement corrosion on the seismic capacity of the case-study building. The pushover curves for both principal directions exhibit a reduction in lateral strength and stiffness relative to the uncorroded condition, consistent with the deterioration mechanisms described in the manuscript. In the longitudinal direction, the yield point occurs at a slightly lower spectral acceleration, and the post-yield plateau shortens, reflecting the reduced elongation capacity of corroded reinforcement and the degradation of concrete cover. In the transversal direction, the impact is even more pronounced: the peak spectral acceleration decreases noticeably, and the onset of post-peak softening occurs earlier, confirming the inherently lower capacity of this direction and its amplified sensitivity to material degradation. These reductions are consistent with the estimated corrosion-induced losses in ductility (10–16%) and the expected weakening of boundary elements and web reinforcement. Figure 6 illustrates the effect of carbonation-induced reinforcement corrosion on the seismic fragility of the case-study structure, showing a clear increase in the probability of exceeding all damage states for both principal directions. The fragility curves shift systematically towards lower PGA values compared to the uncorroded condition, indicating that the building reaches the same damage levels under weaker ground-motion intensities. This behavior is driven by the reductions in ductility, stiffness, and post-yield deformation capacity associated with corrosion, as reflected in the degraded pushover curves.

It has to be mentioned as well that the mean value of the carbonation depth at 50 years evaluated using Equation (7) is about 10 mm for an interior element, a value which is significantly smaller than the one computed using the simplified approach with Equation (6). Thus, it can be observed that the simplified model gives an upper-bound estimate of carbonation depth, while the probabilistic model provides a more realistic range. Using both helps quantify uncertainty in the deterioration process.

The seismic losses, evaluated on a 50,000-year catalog for the Vrancea intermediate-depth seismic source previously defined in [55], for the four sets of fragility functions are reported in Table 10, using the model proposed by Martins and Silva [56]. Table 10 quantifies the impact of carbonation-induced reinforcement corrosion on the seismic loss estimates of the case-study structure. The results clearly show that corrosion leads to an increase in both mean seismic losses and average annual seismic losses in both structural directions, an aspect also observed in other studies (e.g., [4,12,57,58]). In the longitudinal direction, mean losses rise from 3.39% to 4.17%, while annual losses increase from 0.94% to 1.16%, reflecting a moderate but consistent deterioration in performance. The effect is more pronounced in the transversal direction, where the structure is inherently more flexible and vulnerable: mean losses increase from 4.80% to 5.38%, and annual losses rise from 1.33% to 1.49%. This amplification of losses aligns with the reduced stiffness, ductility, and lateral capacity observed in the corrosion-affected pushover curves and fragility functions. Overall, Table 10 demonstrates that even relatively modest levels of carbonation-induced corrosion produce measurable and meaningful increases in seismic risk, highlighting the importance of incorporating deterioration mechanisms into long-term vulnerability and loss assessments for aging RC buildings. While these findings provide a critical benchmark for similar 8-to-12-storey typologies in Bucharest, they should be extrapolated to low-rise RC or masonry structures with caution. Lower-rise buildings, characterized by higher relative stiffness and different dominant failure modes (such as shear-controlled behavior), may exhibit a different sensitivity to material variability and corrosion-induced degradation.

Table 10. Comparison of expected annual losses (EALs) and mean damage ratios for the case-study building in uncorroded and corroded conditions.

Direction	Mean Seismic Loss	Average Annual Seismic Loss
Long.	3.39%	0.94%
Long.-corroded	4.17%	1.16%
Transv.	4.80%	1.33%
Transv.-corroded	5.38%	1.49%

6. Conclusions

The analyses presented in this study synthesize historical evidence, material test data, and probabilistic modeling to evaluate the mechanical properties of concrete and reinforcing steel used in Bucharest's reinforced concrete building stock across multiple construction eras. By integrating archival material datasets, post-earthquake observations, and statistically derived material models, the research provides a comprehensive overview of the factors governing seismic performance at the material level. A case-study structure is employed in order to evaluate the impact of carbonation-induced corrosion on the seismic fragility. The main observations of the study are summarized below:

- Historical reinforcing steels (OB37, TOR47, and PC52) used for buildings in Romania in the 1950–1990 period display distinct strength, ductility, and variability profiles, which must be explicitly reflected in nonlinear modeling.
- In situ concrete strengths for pre-1990 buildings frequently underperform relative to prescribed classes, contributing to elevated seismic vulnerability.

- The pre-1970 RC case-study building exhibits significantly lower capacity in the transversal direction, consistent with observed damage during past Vrancea earthquakes.
- Empirical displacement–capacity relationships confirm limited deformation capacity in the boundary elements.
- Carbonation-induced reinforcement corrosion leads to measurable reductions in stiffness, ductility, and lateral resistance of the case-study structure, even for moderate corrosion levels.
- Incorporating deterioration models shifts the fragility curves toward lower PGA values, indicating earlier onset of damage under seismic loading.
- Seismic loss estimates increase in both directions when corrosion is considered, with greater amplification in the inherently weaker transversal direction.
- The comparison between simplified and probabilistic carbonation models highlights substantial uncertainty in carbonation depth, underlining the need for material-specific data.
- The study demonstrates the necessity of integrating material variability, aging effects, and nonlinear structural behavior into future risk-mitigation and retrofit strategies.
- To mitigate the identified transversal vulnerabilities and the time-dependent effects of corrosion, several retrofitting strategies can be recommended for the Bucharest building stock. The most robust approach for the core wall typology involves RC jacketing of the existing structural walls, which provides both a structural capacity increase and a protective layer against further carbonation. Additionally, the strategic implementation of new transversal shear walls or the use of Fiber-Reinforced Polymers (FRPs) at critical wall boundary regions can effectively restore seismic performance levels.

This study is subject to several limitations stemming from data availability, modeling assumptions, and the scope of the case-study analysis. The historical material datasets used to derive probabilistic models originate from past testing campaigns and archival documents, which may not fully capture the spatial variability and quality inconsistencies across the entire Bucharest building stock. The structural assessment focuses on a single pre-1970 RC building, meaning the findings cannot be universally generalized to other typologies or detailing practices. Simplifications inherent in the equivalent single-degree-of-freedom representation may understate higher-mode and torsional effects, particularly relevant for irregular or taller buildings. The carbonation-induced corrosion modeling relies on assumed environmental exposure, concrete cover conditions, and corrosion rates that may vary in practice, while degradation of bond strength, confinement, and bar buckling is represented through simplified analytical relationships rather than detailed nonlinear modeling. While this study treats the variability of concrete strength and reinforcement degradation as independent probabilistic variables, it is recognized that in situ construction quality often exhibits a correlation; specifically, poor-quality concrete may frequently coincide with inadequate detailing or higher susceptibility to steel corrosion due to increased permeability. Due to the lack of paired historical data in the archives that would allow for the quantification of such a correlation, it was not explicitly implemented in the current framework. Future research should prioritize site-specific multi-parameter testing to establish these statistical correlations, which could further refine the accuracy of time-dependent fragility estimates for the aging building stock. Additionally, although the ground-motion dataset is hazard-consistent for Bucharest, alternative ensembles could produce variations in fragility estimates. Consequently, these limitations highlight the need for expanded material databases and large-scale, multi-building analyses to generalize these findings across the broader spectrum of Bucharest's building stock.

Author Contributions: Conceptualization, F.P. and L.P.F.; methodology, F.P.; software, L.P.F.; validation, F.P.; formal analysis, F.P.; investigation, L.P.F.; resources, L.P.F.; data curation, L.P.F.; writing—original draft preparation, L.P.F.; writing—review and editing, F.P.; visualization, F.P.; supervision, F.P. All authors have read and agreed to the published version of the manuscript.

Funding: This work was supported by Universitatea Tehnica de Constructii Bucuresti, project number GNaC-ARUT-2025-UTCB-3.

Data Availability Statement: The original contributions presented in this study are included in the article. Further inquiries can be directed to the corresponding author.

Conflicts of Interest: The authors declare no conflicts of interest.

References

1. Pavel, F.; Crowley, H.; Romão, X.; Vladut, R.; Pereira, N.; Ozsarac, V. Evolution of National Codes for the Design of RC Structures in Romania. *Bull. Earthq. Eng.* **2023**, *22*, 911–949. [CrossRef]
2. Crowley, H.; Dabbeek, J.; Despotaki, V.; Rodrigues, D.; Martins, L.; Silva, V.; Romão, X.; Pereira, N.; Weatherill, G.; Danciu, L. European Seismic Risk Model—Insights and Emerging Research Topics. In *Proceedings of the Progresses in European Earthquake Engineering and Seismology*; Vacareanu, R., Ionescu, C., Eds.; Springer International Publishing: Cham, Switzerland, 2022; pp. 161–178.
3. Xiao, J.; Li, J.; Zhu, B.; Fan, Z. Experimental Study on Strength and Ductility of Carbonated Concrete Elements. *Constr. Build. Mater.* **2002**, *16*, 187–192. [CrossRef]
4. Diamantopoulos, S.; Achmet, Z.; Stefanidou, S.; Markogiannaki, O.; Fragiadakis, M. Fragility Assessment and Risk-Targeted Design of RC Buildings Considering the Effect of Aging. *Structures* **2024**, *62*, 106277. [CrossRef]
5. Kordtabar, B.; Dehestani, M.; Yazdanpanah, O.; Hasanzadeh, A. Time Dependent Seismic Fragility and Serviceability Assessment of Reinforced Concrete Frames under Chloride Induced Corrosion. *Sci. Rep.* **2025**, *15*, 40575. [CrossRef] [PubMed]
6. Geng, F.; Wen, Z.; Xu, C.; Chau, K.T. Time-Dependent Seismic Fragility for Aging RC Frame Structures in the Inland Atmosphere Environment. *J. Earthq. Eng.* **2023**, *27*, 1440–1457. [CrossRef]
7. Shi, Z.; Liang, Y.; Cao, Y.; Yan, J. Time-Variant Seismic Fragility of Offshore Continuous Beam Bridges Based on Collapse Analysis. *Appl. Sci.* **2020**, *10*, 8595. [CrossRef]
8. Nigro, F.; Zinco, A.; Martinelli, E. A Practice-Oriented Procedure for Seismic Reliability Assessment of RC Structures Affected by Carbonation-Induced Degradation. *Appl. Mech.* **2021**, *2*, 820–840. [CrossRef]
9. Vaezi, H.; Karimi, A.; Shayanfar, M.; Safiey, A. Seismic Performance of Low-Rise Reinforced Concrete Moment Frames under Carbonation Corrosion. *Earthq. Struct.* **2021**, *20*, 215–224.
10. Zheng, X.-W.; Li, H.-N.; Gardoni, P. Probabilistic Seismic Demand Models and Life-Cycle Fragility Estimates for High-Rise Buildings. *J. Struct. Eng.* **2021**, *147*, 04021216. [CrossRef]
11. Sung, Y.-C.; Su, C.-K. Time-Dependent Seismic Fragility Curves on Optimal Retrofitting of Neutralised Reinforced Concrete Bridges. *Struct. Infrastruct. Eng.* **2011**, *7*, 797–805. [CrossRef]
12. Samanta, N.; Dasgupta, K.; Di-Sarno, L.; Prota, A. Effect of Ageing on the Seismic Risk of RC Wall–Frame Buildings under Sequential Earthquakes and Consequences for Insurance Premiums. *Int. J. Disaster Risk Reduct.* **2026**, *135*, 106039. [CrossRef]
13. Pavel, F.; Ioan, P. *Seismic Risk Assessment of Residential Buildings in Bucharest Constructed Before 1990*; Ed.Noua: Bucharest, Romania, 2024.
14. Avram, C. *Reinforced Concrete in Romania*; Ed.Tehnica: Bucharest, Romania, 1987; Volume 2.
15. Carare, T. *High-Grade Steels for Reinforced Concrete and Prestressed Concrete*; Ed.Tehnica: Bucharest, Romania, 1969.
16. Pavel, F.; Vacareanu, R.; Scupin, A. Seismic Fragility Assessment for Post-1977 High-Rise Reinforced Concrete Structures in Romania. *Bull. Earthq. Eng.* **2021**, *19*, 6521–6544. [CrossRef]
17. CEN. *Eurocode 2: Design of Concrete Structures; Part 1-1: General Rules and Rules for Buildings*; CEN: Bruxelles, Belgium, 2004.
18. *STAS 1546-50*; Instructions for the Design of Reinforced Concrete Sections According to the Ultimate Strength Method. Ministry of Constructions and Construction Materials Industry: Bucharest, Romania, 1952.
19. *P8-62*; Design of Concrete, Reinforced Concrete and Prestressed Concrete Elements for Civil and Industrial Constructions. CSCAS: Bucharest, Romania, 1963.
20. *STAS 10107/0-76*; Civil and Industrial Constructions. The Design and Dimensioning of Reinforced Concrete and Prestressed Concrete Elements. Romanian Institute of Standardization: Bucharest, Romania, 1976.
21. *STAS 10107/0-90*; The Design and Dimensioning of Concrete, Reinforced Concrete and Prestressed Concrete Structural Elements. Romanian Institute of Standardization: Bucharest, Romania, 1991.
22. *STAS 438-54*; Hot Rolled Steel. Round Reinforcing Steel. Standardization Comission: Bucharest, Romania, 1955.

23. *STAS 438-61*; Hot Rolled Steel. Round Reinforcing Steel. Standardization Comission: Bucharest, Romania, 1962.
24. *STAS 438/1-80*; Steel Products for Concrete Reinforcement. Hot-Rolled Reinforcing Steel. Grades and Technical Quality Requirements. IRS: București, Romania, 1981.
25. Carare, T.; Vernescu, M.; Dinuliu, R. Research on Reinforcing Steels for Reinforced Concrete. *INCERC Stud. Res.* **1965**, *2*, 43–65.
26. JCSS. *JCSS Probabilistic Model Code*; JCSS: Zürich, Switzerland, 2001.
27. INCERC. *Study on the Application of Mathematical Statistics to the Definition and Quality Control of Construction Materials*; INCERC: Bucharest, Romania, 1991.
28. *P2-62*; Technical Instructions Regarding the Constructive Measires for Masonry Structures in Seismic Areas. State Commitee for Constructions, Architecture and Sistematization: Bucharest, Romania, 1963.
29. *P13-63*; Code for the Design of Civil and Industrial Buildings in Seismic Regions. State Committee for Constructions, Architecture and Sistematization: Bucharest, Romania, 1963.
30. IPCM. *Local Repairs to the Elements Damaged During the 4 March 1977 Earthquake at the ICPET Pavilion, Aimed at Maintaining the Building in Operation*; IPCM: Bucharest, Romania, 1977.
31. Abdullah, S.A.; Wallace, J.W. Drift Capacity of Reinforced Concrete Structural Walls with Special Boundary Elements. *Struct. J.* **2019**, *116*, 183–194. [CrossRef]
32. Pavel, F.; Panfilii, P.; Farsangi, E.N. Estimation of Displacement Capacity of Rectangular RC Shear Walls Using Experimental and Analytical Database. *Stavební Obz. Civ. Eng. J.* **2020**, *29*, 35. [CrossRef]
33. Wood, S.L. Minimum Tensile Reinforcement Requirements in Walls. *Struct. J.* **1989**, *86*, 582–591. [CrossRef]
34. *SeismoStruct—A Computer Program for Static and Dynamic Nonlinear Analysis of Framed Structures*; SeismoSoft: Pavia, Italy, 2020.
35. Mander, J.B.; Priestley, M.J.N.; Park, R. Theoretical Stress-Strain Model for Confined Concrete. *J. Struct. Eng.* **1988**, *114*, 1804–1826. [CrossRef]
36. Menegotto, M.; Pinto, P.E. Method of Analysis for Cyclically Loaded R.C. Plane Frames Including Changes in Geometry and Non-Elastic Behaviour of Elements under Combined Normal Force and Bending. In *Proceedings of the IABSE Symposium of Resistance and Ultimate Deformability of Structures Acted on by Well-Defined Repeated Loads*; IABSE: Zurich, Switzerland, 1973; Volume 13, pp. 15–22.
37. Vamvatsikos, D.; Cornell, C.A. Incremental Dynamic Analysis. *Earthq. Eng. Struct. Dyn.* **2002**, *31*, 491–514. [CrossRef]
38. Pavel, F.; Carale, G. Seismic Assessment for Typical Soft-Storey Reinforced Concrete Structures in Bucharest, Romania. *Int. J. Disaster Risk Reduct.* **2019**, *41*, 101332. [CrossRef]
39. Nica, G.-B.; Pavel, F.; Hojda, G. A Fast Nonlinear Dynamic Analysis Automated Approach to Produce Fragility Curves for 3D RC Frames. *Eng. Struct.* **2023**, *281*, 115695. [CrossRef]
40. Crowley, H. European Exposure and Vulnerability Models: State-of-The-Practice, Challenges and Future Directions. In *Advances in Assessment and Modeling of Earthquake Loss*; Akkar, S., Ilki, A., Goksu, C., Erdik, M., Eds.; Springer International Publishing: Cham, Switzerland, 2021; pp. 155–168.
41. Rodríguez, J.; Andrade, C. *CONTECVET A Validated Users Manual for Assessing the Residual Service Life of Concrete Structures*; GEOCISA and Torroja Institute: Madrid, Spain, 2001.
42. Kashani, M.M.; Crewe, A.J.; Alexander, N.A. Nonlinear Stress–Strain Behaviour of Corrosion-Damaged Reinforcing Bars Including Inelastic Buckling. *Eng. Struct.* **2013**, *48*, 417–429. [CrossRef]
43. FIB. *FIB Model Code for Concrete Structures 2020*; Fédération Internationale du Béton: Lausanne, Switzerland, 2024.
44. FIB. *FIB Bulletin 34—Model Code for Service Life Design*; International Federation for Structural Concrete: Lausanne, Switzerland, 2006.
45. FIB. *FIB Model Code for Concrete Structures 2010*; Fédération Internationale du Béton: Lausanne, Switzerland, 2013.
46. Ghosh, J.; Padgett, J.E. Aging Considerations in the Development of Time-Dependent Seismic Fragility Curves. *J. Struct. Eng.* **2010**, *136*, 1497–1511. [CrossRef]
47. Dhakal, R.P.; Maekawa, K. Reinforcement Stability and Fracture of Cover Concrete in Reinforced Concrete Members. *J. Struct. Eng.* **2002**, *128*, 1253–1262. [CrossRef]
48. Monti, G.; Nuti, C. Nonlinear Cyclic Behavior of Reinforcing Bars Including Buckling. *J. Struct. Eng.* **1992**, *118*, 3268–3284. [CrossRef]
49. Massone, L.M.; López, E.E. Modeling of Reinforcement Global Buckling in RC Elements. *Eng. Struct.* **2014**, *59*, 484–494. [CrossRef]
50. Yang, H.; Sun, P.; Deng, Y. Experiment Investigation of the Influence of Reinforcing Bar Buckling on Seismic Behavior of RC Columns. *Eng. Struct.* **2020**, *220*, 110923. [CrossRef]
51. Coronelli, D.; Gambarova, P. Structural Assessment of Corroded Reinforced Concrete Beams: Modeling Guidelines. *J. Struct. Eng.* **2004**, *130*, 1214–1224. [CrossRef]
52. Georgescu, D.; Apostu, A.; Gavrilescu, R. Experimental research, essential component in the application of different methods to establish the service life of concrete structures. *Rom. J. Mater.* **2011**, *3*, 219–228.

53. Moraru, M.C. *Application of Descriptive and Performance-Based Methods in Ensuring the Durability of Concrete Elements and Structures Made with Blended Cements*; Technical University of Civil Engineering Bucharest: Bucharest, Romania, 2021.
54. Melchers, R.; Beck, A. *Structural Reliability Analysis and Prediction*, 3rd ed.; John Wiley & Sons: Hoboken, NJ, USA, 2018.
55. Pavel, F.; Vacareanu, R.; Calotescu, I.; Sandulescu, A.-M.; Arion, C.; Neagu, C. Impact of Spatial Correlation of Ground Motions on Seismic Damage for Residential Buildings in Bucharest, Romania. *Nat. Hazards* **2017**, *87*, 1167–1187. [CrossRef]
56. Martins, L.; Silva, V. Development of a Fragility and Vulnerability Model for Global Seismic Risk Analyses. *Bull. Earthq. Eng.* **2021**, *19*, 6719–6745. [CrossRef]
57. Karapetrou, S.T.; Fotopoulou, S.D.; Pitilakis, K.D. Seismic Vulnerability of RC Buildings under the Effect of Aging. *Procedia Environ. Sci.* **2017**, *38*, 461–468. [CrossRef]
58. Hasanzadeh, R.; Ahmadi, J.; Eghbali, M.; Samadian, D.; Salmanmohajer, H. Reduction of Seismic Resiliency of RC Structures Caused by Chloride Corrosion for Typical School Buildings Located in Hot Climates. *Structures* **2021**, *34*, 4060–4076. [CrossRef]